Miscible displacement of a layer with finite width in porous media

Ching-Yao Chen and Shu-Wei Wang
Department of Mechanical Engineering, Da-Yeh University, Chan-Haw, Taiwan, ROC

Keywords *Numerical simulation, Flow, Porous media*

Received April 2001
Revised August 2001
Accepted August 2001

Abstract *Miscible displacement of a more viscous finite layer in porous media is simulated by means of high accuracy numerical schemes. Viscous fingers on the trailing front where the mobility ratio is unfavorable are found to catch up, however they never break through the stable leading front. Two stages of fingering orientation are observed. At an earlier time when the influences of finite thickness of the layer are not yet fully realized, the fingers move forward with the similar features to the conventional fingering findings. However, these fingering patterns are redirected upstream after the arrival of most of fingers to the leading front. The leading front remains stable with strong dispersion effects and moves nearly constantly with original displacing velocity. The growth rate of the layer thickness depends strongly on the viscosity ratio.*

I. Introduction

The subject of porous media flows involving fluids of different viscosities has been studied extensively for several decades. Accurate predictive abilities for displacements in porous media represent a prerequisite for addressing a host of problems in fields such as hydrology, enhanced oil recovery or underwater pollution contamination. The exploration of fingering instability governed by the effects of viscosity contrast has been an ongoing research subject as well, dating back to the pioneering experiments of Hill (1952) and Saffman and Taylor (1958). Traditionally, most of the analytical, experimental and numerical investigations in this area have been performed for the displacement process on a semi-infinite length of more viscous environment, cf. the recent reviews by Homsy (1987), Yortsos (1990) and McCloud and Maher (1995). However, the finite layer confined by the less viscous fluids, present in many applications, to our knowledge has not yet been explored. The catch-up of viscous fingers triggered on the trailing edge, where the viscosity ratio is unfavorable, might lead to interesting mechanism such that if the fingers would break through the layer and evolve channels within it or growth of the fingers are subdued on the frontal boundary. The main objective in the present investigation lies in the exploration of the influences of layer's finite thickness and fingering patterns of the flow field. We pursue this goal by means of highly accurate direct numerical simulations, which resolved all the relevant length scales without introducing significant levels of numerical diffusion.

Ching Yao Chen would like to express appreciation to Professor Meiburg for his continuous advice and encouragement to the research. Support by a ROC NSC Research Grant 89-2212-E-212-036 is gratefully acknowledged.

As far as the miscible displacement of layer of finite thickness is concerned, some guidance can be obtained from simulations of infinite flows. A first known finite difference algorithm for simulating an unstable miscible displacement was developed by Peaceman and Rachfird (1962). More recent high-accuracy time-dependent simulation by Tan and Homsy (1988) provides more detailed information. Using a Fourier spectral method, Tan and Homsy (1988) explored the miscible fingering dynamics as a function of the mobility ratio and the Peclet number, and found good agreement with the growth rates of their earlier linear stability analysis (Tan and Homsy, 1986). The nonlinear mechanism, such as spreading, shielding, merging and tip-splitting were observed and can be best understood in terms of the underlying vorticity dynamics. The finite difference simulations by Christie and Bond (1987) and Christie (1989) exhibited similar fingering dynamics and yielded good global quantitative agreement with experimental recovery data by Blackwell *et al.* (1959). Some other numerical simulations, e.g. Sherwood (1987), Fayers *et al.* (1992) and Bratvedt *et al.* (1992), choose not to account for the molecular diffusion, so that the computational grid has to provide the short-wavelength cutoff via numerical diffusion. Rogerson and Meiburg (1993a) extended the stability analysis for flows involving shear across the interface, and observed a stabilize effect by the shear. This shear stabilization was confirmed by the same authors (Rogerson and Meiburg, 1993b) numerically. More recently, Lajeunesse *et al.* (1999) studied the downward displacement at very high rates for diffusive effect to be negligible both experimentally and theoretically. A formation of a two-dimensional tongue of injected fluid resulted under certain conditions on the viscosity ratio and flow rate. Ruith and Meiburg (2000) and Camhi *et al.* (2000) simulated the displacements with gravity override. The authors discovered that the coupling between viscosity and gravity is predominantly one way, in that the gravity can amplify the viscosity vorticity, but not vice versa. Chen *et al.* (2001) studied the motion of miscible droplet. The droplet shape was investigated and also the influences of the dynamic surface tension (Korteweg stresses). They reported the negative frontal curvature was found to stabilize the unfavorable mobility ratio on the more viscous droplet.

Other work highly relevant to the present study is that dealing with when the viscosity-concentration relationship is non-monotonic, investigated by Manickam and Homsy (1993, 1994, 1995) and Pankiewitz and Meiburg (1999). The non-monotonic viscosity variation develops an unstable zone followed downstream by a stable zone. This downstream stable zone, which is similar to the leading mixing front with favorable viscosity ratio in present situation, acts as a barrier to the growth of fingering instabilities. Manickam and Homsy (1993) found that typical quadrupole structures of the flow field resulted from the non-monotonic viscosity profiles, as opposed to the dipole observed for the monotonic variation. In general, according to Manickam and Homsy, the instabilities are more pronounced as the end-point viscosity contrast becomes more unfavorable; the increase of maximum viscosity stabilizes displacements with an unfavorable end-point viscosity contrast, while destabilizing with a

favorable one. The results of stability analysis are confirmed by the followed up numerical simulations, cf. Manickam and Homsy (1994). The phenomenon of "reverse fingering", during which the fingers tend to propagate backwards when viewed in a reference frame moving with the front, were observed in the simulations caused by the barrier to the forward growth of fingers. Similar analysis and simulations in the geometries of radial flow and quarter five-spot configuration were studied by Pankiewitz and Meiburg (1999). Contrasted to rectilinear displacement, it was found that, for a given end-point viscosity ratio, whether the overall viscosity contrast is favorable or not, an increase in the maximum viscosity generally leads to a more unstable front. Manickam and Homsy (1995) analyzed the cases of vertical flow with monotonic viscosity profiles, and horizontal flows with non-monotonic viscosity profiles, and found great similarities in the two situations. Reverse fingering was also observed in a density-driven displacement with a favorable viscosity ratio.

Here, detailed miscible displacement simulations of a finite layer will yield qualitative and quantitative information essential for correctly anticipating groundwater hydrology, as well as for assessing the effectiveness of strategies for groundwater contamination. Control parameters, such as viscosity ratios and dimensionless flow rates (Peclet number) are simulated systematically. The outline of this paper is as follows. After formulating the physical problem and providing a brief review of the computational technique in Section II, Section III will focus on the computational results and their interpretation. Conclusions will be provided in Section IV.

II. Physical problem and governing equations

We consider the physical problem of time-dependent displacement of a more viscous miscible fluid confined within a layer with width W in a rectangular domain, such as the one depicted in Figure 1. The layer is displaced by the surrounding less-viscous fluid with a uniform velocity U. The governing

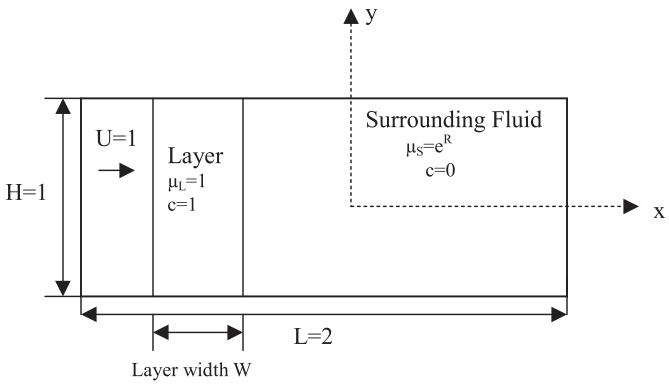

Note: In a rectangular domain, a finite thickness layer is displaced by a less viscous surrounding fluid with a uniform velocity U

Figure 1.
Principal sketch

equations in a homogeneous porous medium of permeability k take the forms:

$$\nabla \cdot \mathbf{u} = 0 \tag{1}$$

$$\nabla p = -\frac{\mu}{k}\mathbf{u} \tag{2}$$

$$\frac{\partial c}{\partial t} + \nabla \cdot (\mathbf{u}c) = D\nabla^2 c. \tag{3}$$

Here, $\mathbf{u}$ denotes the velocity, c the concentration of fluid in the layer, D the diffusion coefficient and p the pressure. Viscosity is indicated by μ. The expression of a scalar diffusion coefficient D represents a relatively crude approximation of real dispersion mechanism inside a porous medium. However for lack of a better model, as discussion and references given by Petitjeans *et al.* (1999), a scalar diffusion coefficient is the best to be employed for now, in order not to occlude the identifiable physical mechanism at work.

In order to render the governing equations dimensionless, we take the vertical extent H of the flow domain as the characteristic length scale and k a typical permeability value. The nominal displacing velocity U serves as the velocity scale, thus time scale H/U. By furthermore scaling with viscosity of layer μ_L, where the subscript L indicates the fluid in the layer, and pressure $\mu_L UH/k$, we define the dependence of viscosity-concentration has the form (Tan and Homsy, 1988; Chen and Meiburg, 1998a, b):

$$\mu(c) = e^{R(1-c)}, \tag{4}$$

which R is the viscosity control parameter that determines the viscosity ratio as e^R. The momentum equation can be recast into a vorticity (ω) and streamfunction (ψ) formulation (Ruith and Meiburg, 1999):

$$\omega = \frac{\partial v}{\partial x} - \frac{\partial u}{\partial y} \tag{5}$$

$$u = 1 + \frac{\partial \psi}{\partial y} \quad , \quad v = -\frac{\partial \psi}{\partial x}. \tag{6}$$

It should be noticed that the streamfunction mentioned here represents purely the component caused by the generation of vorticity in the original irrotational He-le-Shaw flow. In order not to confuse with the overall streamfunction that includes uniform base flow, we refer to perturbation streamfunction in the following. The dimensionless momentum and concentration equations are obtained:

$$\nabla^2 \psi = -\omega \tag{7}$$

$$\omega = -R\nabla\psi \cdot \nabla c \tag{8}$$

$$\frac{\partial c}{\partial t} + \mathbf{u} \cdot \nabla c = \frac{1}{Pe}\nabla^2 c \tag{9}$$

where the Peclet number Pe is the form:

$$Pe = \frac{UH}{D}. \tag{10}$$

Boundary conditions are prescribed as follows (Ruith and Meiburg, 1999):

$$x = in/out\ flow \quad : \ \frac{\partial \psi}{\partial x} = 0 \ , \ \frac{\partial \omega}{\partial x} = 0 \ , \ \frac{\partial c}{\partial x} = 0 \tag{11}$$

$$y = \pm 0.5 \quad : \ \psi = 0 \ , \ \frac{\partial c}{\partial y} = 0. \tag{12}$$

The numerical code is largely identical to one used for earlier investigation by Ruith and Meiburg (2000). The Poisson equation of streamfunction is solved by a spectral method with a Galerkin-type discretization of cosine expansions in the stream-wise direction, accompanied by sixth order compact finite difference in the normal direction. Third order Runge-Kutta method is applied to obtain the temporal concentration distribution. The code is validated by comparing the growth rates with the values obtained from linear stability theory in a plane front with semi-infinite layer, i.e. $W = \infty$. More details on the implementation of these schemes are provided by Meiburg and Chen (2000), as well as Ruith and Meiburg (2000).

III. Results

We start by describing the temporal and spatial evolution of a reference case, in order to identify the dominant mechanisms at work. Subsequently, the values of the governing parameters will be varied individually, in order to elucidate their effects.

III.A Reference cases

A representative calculation for $R = -2.5$, Pe = 2,000 and W = 0.125 is described. The computational domain extends over the range of (–1,1) and the rear contacting mixing interface is placed at x = –0.75. The R-value indicates that the layer is displaced within an about 12 times less viscous environment. Figure 2 displays the time sequences of the concentration fields. At the rear mixing interface, the mobility ratio is unfavorable, and as a result vigorous fingering instability is observed and less viscous fluids penetrate into the more viscous layer. These fingers initially display some of the familiar dynamic behavior, i.e. splitting, merging, etc., cf. Tan and Homsy (1988). As these

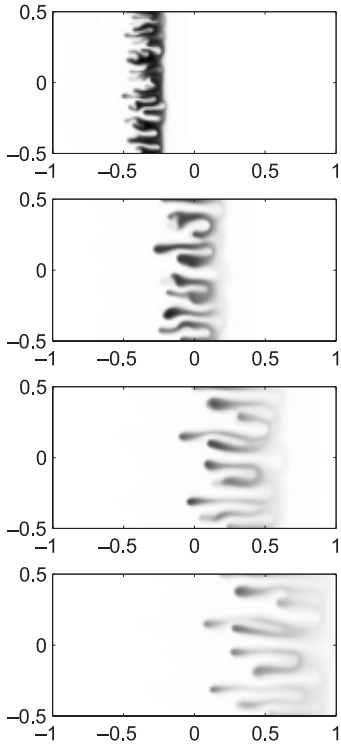

Figure 2.
Reference case: $PE = 2{,}000$; $R = -2.5$ and $W = 0.125$

Note: Concentration contours are shown for times t=0.4, 0.8, 1.2 and t =1.523. Conventional forward fingers are seen at t=0.4. However, reverse fingers evolve after the arrivals of fingers to leading front after t=0.8

penetrated fingers proceed near the leading interface, instabilities are subdued and penetrated fingers never break through the interface. The leading interface moves stably with a nearly constant speed. The stable leading interface can be understood by its viscosity contrast. Locally, the stable mobility ratio results in a flat leading front that moves slower than the less viscous penetrating fingers catching from behind. A very thin area with significant concentration gradient of more viscous fluid is sandwiched by the penetrating finger and the surrounding less-viscous fluid. The high favorable concentration gradient provides strong stable effects, and prevents the continuous growth of fingerings. The penetrating fingers are forced to decelerate and allow more time for dispersion to proceed. Consequently, a highly-mixed region is formed on the leading front. The mixture in the region is more viscous, and therefore displaces the surrounding fluid in a stable path.

One interesting point is that fingering reorientation is observed after most of the penetrating fingers reach near the leading interface. In situations where the influences of finite width are not significant, such as conventional semi-infinite displacements (Tan and Homsy, 1988; Ruith and Meiburg, 1999) or

wider layer $W = 0.5$ at t = 0.8 shown in Figure 3, the fingers move forward with round tip fronts and relatively irregular roots. The vorticity peaks, with a typical dipole structures, appear at the fingers' tips with similar shapes to the concentration images. The perturbation streamlines show a double eddy pair within each finger and face downstream. At current situation of thin layer, while a few fingers penetrate nearly the leading interface at early time t = 0.4, the influences of finite thickness have not yet been fully realized by the flow. The flow pattern basically resembles the conventional forward fingerings as described above. However, once most of fingers have reached the leading interface at t = 0.8, the stable front resists the continuous penetration of less viscous fluids and force these forward fingers to reverse their orientation backward, or the reverse fingers which also were observed by Manickam and Homsy (1994, 1995) in a non-monotonic viscosity profiles. The vorticity contours, shown in Figure 4, clearly show that the local peaks are located on the original fingers' roots with the typical rounder shapes. The generation of reverse fingers is even pronounced at later time t = 1.523 that the vorticity distribution appears exactly the same as if the displacement proceeds from the opposite direction. The formation of double-eddy pairs facing upstream for the corresponding perturbation streamlines, also shown in Figure 4, confirms the behavior of reverse fingering due to the finite thickness of more viscous layer.

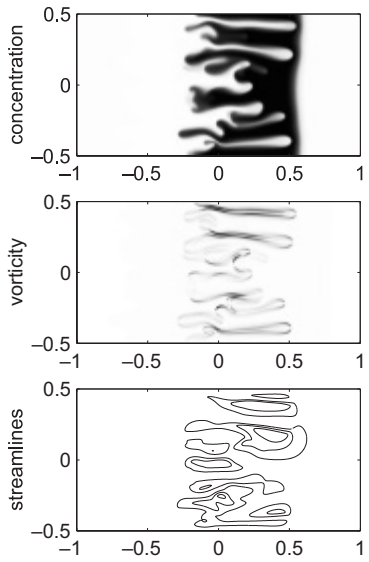

Note: Concentration (top), Vorticity (middle) and perturbation streamfunction (bottom) fields at time=0.8. Features of conventional forward fingers, that both the pairs of vorticity peaks and eddies of streamlines occur at the downstream direction, are observed

Figure 3.
$Pe = 2{,}000$; $R = -2.5$ and $W = 0.5$

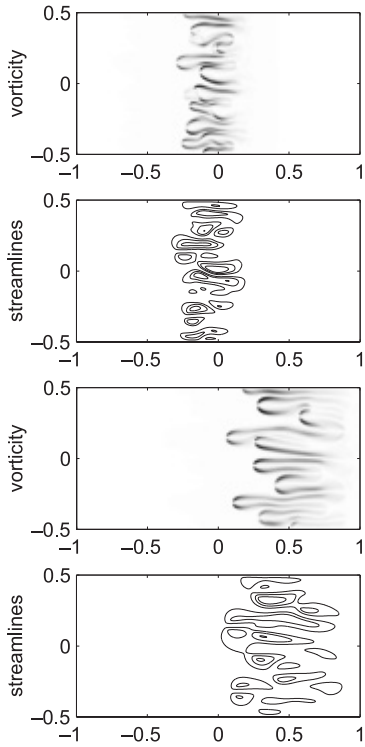

Figure 4.
Reference case: vorticity and perturbation streamfunction fields at times $t = 0.8$ and $t = 1.523$

Note: Features of reverse fingers, that the pairs of vorticity peaks and eddies of streamlines face backward, are clearly seen

Some interesting comparisons can be made between the current findings of reverse fingers to those found in non-monotonic viscosity profiles, cf. Manickam and Homsy (1994, 1995). The basic mechanism of viscous stabilities are similar for both cases, in which a maximum viscosity is placed in between less viscous regions. At the back region of maximum viscosity is a viscous unstable zone, while the front is stable. Thus, similar reverse fingering behaviors resulted. However, the non-monotonic viscosity profiles differ from the current situation on concentration distribution, therefore the effects of diffusion as well. Under the non-monotonic viscosity profile, the unstable-stable distribution of viscosity profiles exists at all times, as long as concentration variation, and leads to the typical quadrupole structures on the contacting front. On the other side, at present condition, even the leading front, in which the variation of viscosity is non-monotonic due to the sandwiched concentration distribution, acts as a barrier and triggers reverse fingering; the diffusion quickly reduces the concentration gradients. Almost no generation of vorticity is observed in this region. The growth of reverse fingers takes place at the roots of the initially forward fingers, where the

viscosity variation is monotonic by definition. The structures of vorticity and perturbation streamfunction appear the typical dipole formation.

The propagating velocity of the more viscous layer, that can be represented by the process time t_b when the concentration contour $c = 0.01$ of leading front reaches the outflow boundary, and dispersed layer width W_d, which is defined as the distance between the points at which average concentration $c_a = 0.01$, in which:

$$c_a(x) = \int_{-0.5}^{0.5} c(x,y)dy, \tag{13}$$

represent quantities of significantly practical interests regarding pollution contamination. Compared to t_b = 1.524 (not shown here) for a passive displacement, $R = 0$, the layer moves in almost the same path with t_b = 1.523 at the present viscosity contrast. It reflects that the stable leading front prevents the breakthrough of the penetrating fingers, and moves insensitively to the viscosity difference on the trailing interface. Dispersed width, normalized by initial width is depicted in Figure 5. For a stable displacement process, the elongation of dispersed width is solely caused by the diffusion within the mixing layer and should remain nearly the same. The instability of trailing front leads to the penetration of viscous fingers at current situation, dispersed width is therefore elongated. However, the continuous growth of dispersed width reflects no breakthrough of the less

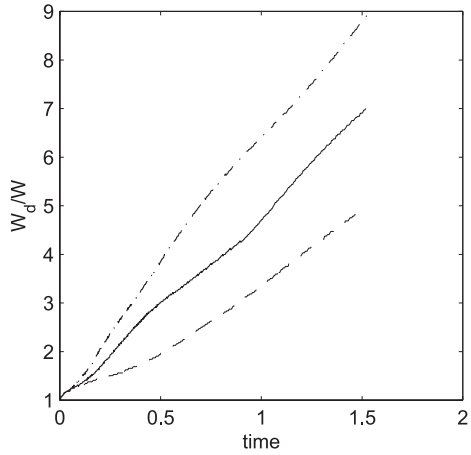

Figure 5.
Pe = 2,000 and W = 0.125. The temporal evolution of dispersed layer width $W_d(t)$ for R = –1.5 (dash); –2.5 (bold) and –3.5 (dash-dot)

Note: The growth of W_d is faster at higher viscosity parameter R. Two stages of dispersed width growth rate can be clearly identified for lower R= –1.5, that is smaller at earlier time (up to about t=0.4), which reflects the continuous penetration of forward fingers. The development of reverse fingers at later stage stretches the layer and causes a faster growth. These two regimes are less distinguishable for higher R due to the sooner arrival of forward fingers to leading front, therefore the earlier appearance of reverse fingers

viscous fluid. Of further interest, for example if chemical reactions between the two miscible fluids are to be considered, is the length of the interfacial region separating the two components, and defined by Chen and Meiburg (1998a, b) as:

$$L(t) = \int_{-0.5}^{0.5} \int_{-1}^{1} ((\frac{\partial c}{\partial x})^2 + (\frac{\partial c}{\partial y})^2)^{\frac{1}{2}} \, dx \, dy \tag{14}$$

and shown in Figure 6. L grows rapidly soon after that the displacement triggers vigorous fingering instability on the trailing front. However, after about $t = 0.3$, the penetrating forward fingers start to reach the stable leading front, fingerings are suppressed, for reasons stated above and strong dispersion takes place. The mixing interfacial length declines significantly due to the strong mixing within the layer.

III.B Effect of viscosity parameter R

The influences of the viscosity parameter will be analyzed by conducting a series of simulations with different values of R, while keeping the other parameters at their respective values of the reference case. The typical viscosity contrast in practical situation between the fluids can vary from $O(1)$ ($R \geq -2.3$), i.e. light chemical component and the groundwater, to $O(10)$ ($R < -2.3$) such as heavy crude oil. For the case of a weak viscosity contrast $R = -1.5$ (cf. Figure 7), the transition of fingering redirection is even more apparent. The lower viscosity contrast causes the fingers to move more slowly compared to the reference case. At $t = 0.4$, all the fingers

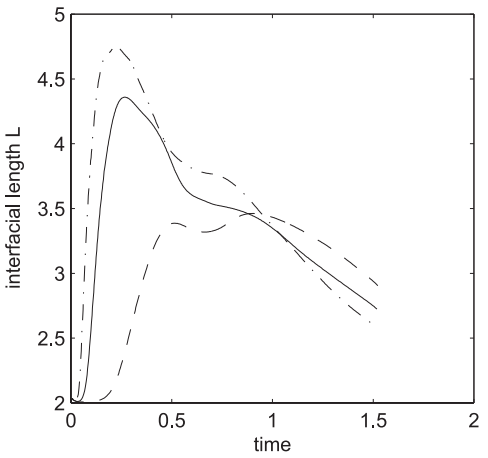

Figure 6.
Pe = 2,000 and W = 0.125. The temporal evolution of interfacial length $L(t)$ for r = –1.5 (dot); –2.5 (bold) and –3.5 (dash-dot)

Note: More rapid growth and higher maximum occur at higher R-value because of more vigorous fingering instability at earlier times. However, due to the sooner arrival to the stable leading front and stabilizing the forward fingers, the mixing interfacial length starts to decline earlier for higher R-value

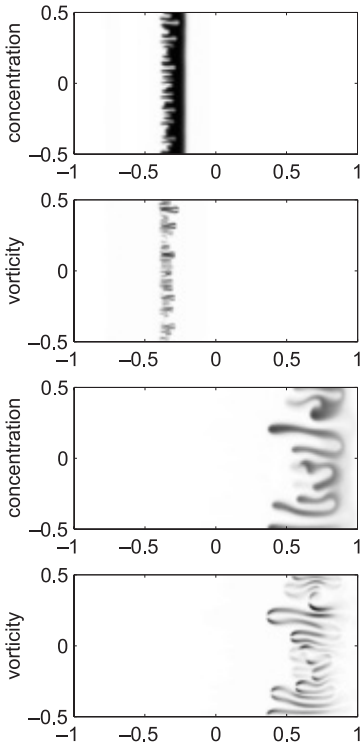

Figure 7.
Pe = 2,000; R = –1.5 and W = 0.125

Note: Concentration and vorticity fields at times t=0.4 and t_b=1.525. Forward fingers and reverse fingers can be identified at early and later times, respectively

have not reached the leading interface yet, and both the concentration and vorticity fields appear to have the typical features of conventional forward fingers, such as rounder tips with local maximum of vorticity dipole pairs at downstream. After the fingers reach the leading interface, the fingers' orientation is reversed, so that the vorticity dipole pairs face upstream, as shown at t_b = 1.525. More numbers and thinner reverse fingers are observed for higher R = –3.5, Figure 8, and process time is about t_b = 1.529. The increment of dispersed width is found more significantly at larger viscosity contrast, shown in Figure 5, that is, resulting from the more vigorous fingering instability and thus quicker and stronger penetration of the less viscous fluid. While higher growth rates of dispersed width result from larger R-value, the process times are nearly the same for all the viscosity differences, as the reason mentioned in the reference case. Two stages of dispersed width growth rate can be clearly identified for lower R = –1.5. The growth rate shows smaller at earlier time (up to about t = 0.4), which reflects the continuous penetration of forward fingers. The advance of stable leading front, associated with the development of reverse fingers at

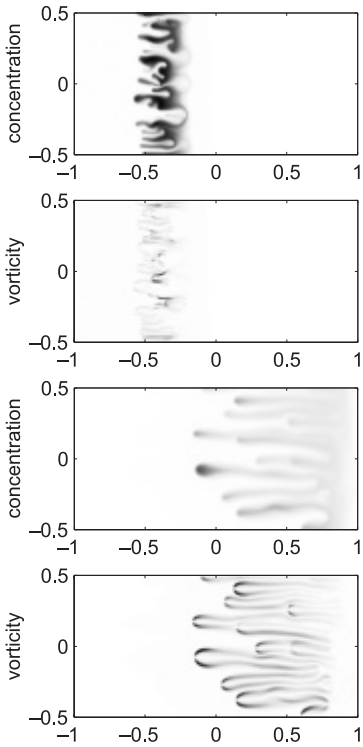

Figure 8.
Pe = 2,000; R = –3.5 and W = 0.125

Note: Concentration and vorticity fields at times t=0.4 and t_b=1.529. Reverse fingers are more pronounced at current higher viscosity ratio

later stage, stretches the layer and causes a faster growth. These two regimes are less distinguishable for higher R due to the sooner arrival of forward fingers to leading front, therefore the earlier appearance of reverse fingers. Influences of various viscosity contrasts to the contacting interface are displayed in Figure 6. More rapid growth and higher maximum occur at higher R-value because of more vigorous fingering instability at earlier times. However, due to the sooner arrival to the stable leading front of the forward fingers, fingering instability is suppressed with significant dispersion. The mixing interfacial length, that depends on the concentration gradient by its definition, starts to decline at earlier time for higher R-value.

III.C Influence of dimensionless flow rate Pe

For a certain fluid combination, the value of Pe is directly proportional to the global displacing flow rate. For a practical displacement process, the value of Pe number based on pure diffusive effect could easily reach more than millions. However, the more realistic dispersion, that is strongly related to

local velocity such as Taylor dispersion (Taylor, 1953) and model has not yet been well established (Petitjeans *et al.*, 1999), is considered, the magnitude of *Pe* could be reduced extremely. Due to the reason as well as the limitation of numerical ability, the range of *Pe*-value simulated here is not beyond $6x10^3$. Depicted in Figure 9 are the concentration and vorticity contours for $Pe = 1,000$ at $t = 0.4$ and t_b = 1.495. Compared to the reference case, less fingering instabilities are triggered with more significant mixing. Different fingering orientation can be also observed from the vorticity contours. While the features of forward finger, that rounder vorticity peaks appear at leading front, can still be partially identified at early time $t = 0.4$, formation of entirely reverse fingering behavior resulted at t_b = 1.495. For higher Pe = 6,000, more numbers of extraordinary fine structures and the apparent reverse fingers as well, are observed as shown in Figure 10. These reverse fingers are considerably longer and slimmer than the lower Peclet number cases. The influences of *Pe* to the process times t_b, dispersed length W_d and interfacial length L are displayed in Figures 11, 12 and 13 respectively. Longer process time is needed for higher *Pe* which represents larger flow rate,

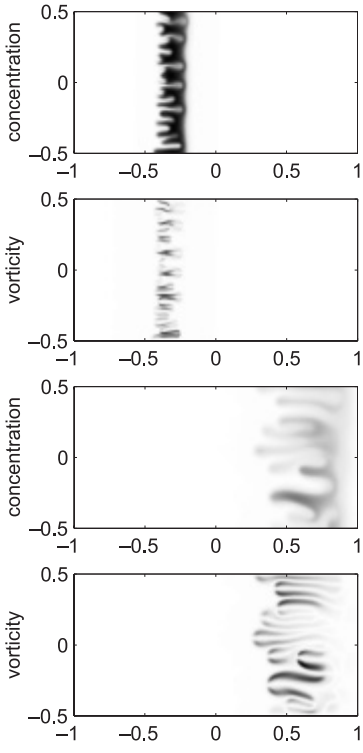

Figure 9.
Pe = 1,000; *R* = –2.5 and *W* = 0.125. Concentration and vorticity fields at times t = 0.4 and t_b = 1.495

Note: The lower *Pe*-value leads to more significant mixing. The process time t_b is earlier than the reference case

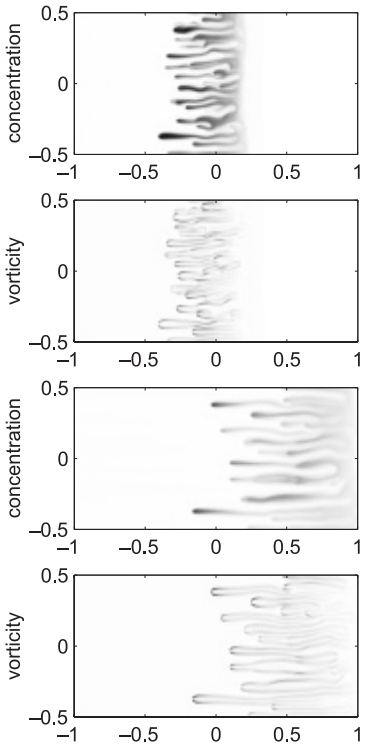

Figure 10.
Pe = 6,000; R = –2.5 and W = 0. 125

Note: Concentration and vorticity fields at times t=0.8 and t_b=1.567. Slimmer and more numbers of reverse fingers resulted from higher Pe

cf. Figure 11, for the range of Peclet values simulated here. It indicates the movement of the stable leading front is characterized by the diffusion. With nearly the same convective effect to the stable leading front, the nature of stronger dispersion for the low Pe-value leads to the sooner arrival of leading front to the numerical boundary. The increase of the dispersed width is determined both by the convective elongation which characterizes the fingering, and diffusive propagation. For convective effect, more significant reverse fingering at higher Peclet number stretches the layer upstream. On the other hand, the stronger diffusion at lower Peclet number increases the thickness of dispersion area on the leading front. Even though the growth of mixing length is higher for higher Peclet number, dependence is not very significant, cf. Figure 12. The higher mixing length due to stronger reverse fingering behaviors associated with longer process time at high Pe-value, suggests a better displacement process in a lower Pe-value if pollutant contamination of the least area, as well as the shortest process time are considered. Interfacial lengths are found higher at larger displacing rates or higher Pe, Figure 13, because of more vigorous fingerings and less mixings.

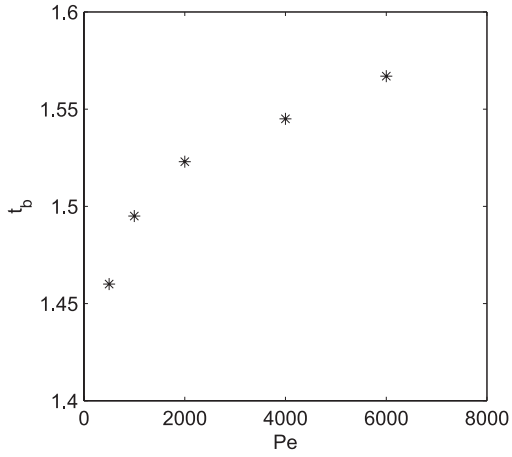

Note: Longer displacement process time t_b is found at higher *Pe*-value due to less dispersion of the stable leading front

Figure 11.
$Re = -2.5$ and $W = 0.125$

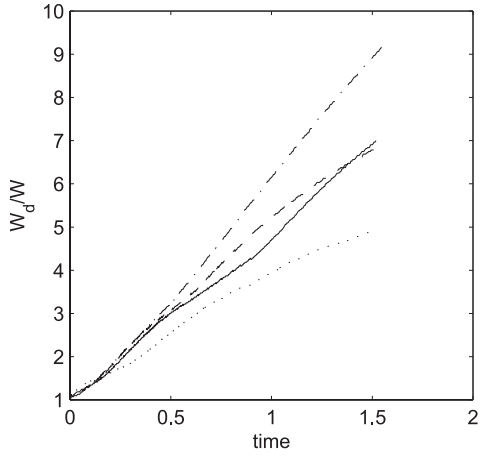

Note: More significant reverse fingering at higher Peclet number stretches the thickness of layer upstream. On the other hand the stronger diffusion at lower Peclet number increases the thickness of dispersion area on the leading front. Even though the growth of mixing length is higher for higher Peclet number, dependence is not very significant

Figure 12.
$R = -2.5$ and $W = 0.125$. The temporal evolution of dispersed layer width $W_d(t)$ for Pe = 1,000 (dash); 2,000 (bold); 4,000 (dot) and 6,000 (dash-dot)

However, maximum interfacial lengths are reached at about the same times, reflecting that arrivals of the forward fingers to the leading front also take nearly the same times for various Peclet numbers. This fact is also confirmed by the very close growth rates of dispersion lengths for different *Pe*-value at earlier times.

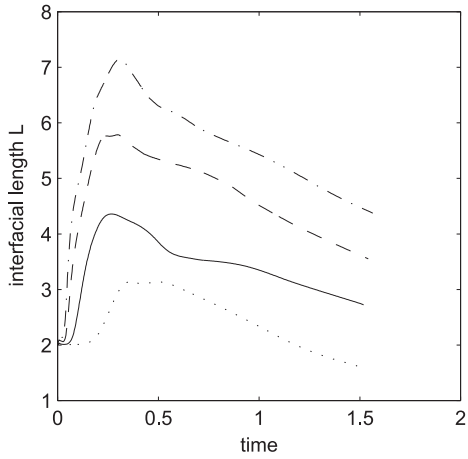

Figure 13.
$R = -2.5$ and $W = 0.125$. The temporal evolution of interfacila length $L(t)$ for Pe = 1,000 (dash); 2,000 (bold); 4,000 (dot) and 6,000 (dash-dot)

Note: Interfacial lengths are found higher at larger displacing rates because of more vigorous fingerings and less mixings. However, maximum interfacial lengths are reached at about the same times that indicates the arrivals of forward fingers to the leading front at nearly the same times for different Peclet numbers

IV. Conclusions

We have presented the numerical simulations of miscible displacement for a finite more viscous layer confined by the less viscous fluids by means of highly accurate numerical schemes. Vigorous fingering instability is triggered on the upstream front due to the unfavorable viscosity ratio locally, and the downstream contacting front remains stable as expected. The influences of finite thickness lead to the reorientation of fingering formation. While at early stage, the fingers have not yet fully arrived the stable leading front (similar to the conventional fingering investigations for semi-infinite more viscous fluids) the fingers travel forward with the features of rounder frontal shapes. The vorticity contours appear dipole pairs with similar shapes to the concentration fingers and local vorticity peaks locate on the tip area. A double eddy formation facing downstream is observed to accelerate the fingers movement. However, the growth of fingers is suppressed once most of the fingers have caught up the stable front. These forward fingers can never break through the resistance of stable front and are forced to redirect. Reverse fingers, similar to Manickam and Homsy (1993, 1994, 1995) are observed. The stable leading front associated with growth of reverse fingers stretch the length of the layer significantly. Similar results are also found in the radial flow fields, in spite of continuous thinning effect to the thickness of annulus due to the radial transportation.

References

Blackwell, R.J., Rayne, J.R. and Terry, W.M. (1959), "Factors influencing the efficiency of miscible displacement", Trans. AIME, Vol. 216, p. 1.

Bratvedt, F., Bratvedt, K., Buchholtz, C.F., Holden, L., Holden, H. and Risebro, N.H. (1992), "A new front-tracking method for reservoir simulation", *SPE Res. Engng*, February, p. 107.

Camhi, E., Meiburg, E. and Ruith, M. (2000), "Miscible rectilinear displacements with gravity override. Part 2: heterogeneous porous media", *J. Fluid Mech.*, Vol. 420, p. 225.

Chen, C.-Y. and Meiburg, E. (1998a), "Miscible porous media displacements in the quarter five-spot configuration. Part 1: the homogeneous case", *J. Fluid Mech.*, Vol. 371, p. 233.

Chen, C.-Y. and Meiburg, E. (1998b), "Miscible porous media displacements in the quarter five-spot configuration. Part 2: effect of heterogeneities", *J. Fluid Mech.*, Vol. 371, p. 269.

Chen, C.-Y., Wang, L. and Meiburg, E. (2001), "Miscible droplets in a porous medium and the effects of Korteweg stresses", *Phys. Fluids* (forthcoming).

Christie, M.A. (1989), "High-resolution simulation of unstable flows in porous media", *SPE Res. Engng*, August, p. 297.

Christie, M.A. and Bond, D.J. (1987), "Detailed simulation of unstable processes in miscible flooding", *SPE Res. Engng*, November, p. 514.

Fayers, F.J., Blunt, M.J. and Christie, M.A. (1992), "Comparison of empirical viscous fingering models and their calibration for the heterogeneous problems", *SPE Res. Engng*, May, p. 195.

Hill, S. (1952), "Channeling in packed columns", *Chem. Engng Sci.*, Vol. 1, p. 247

Hill, S. (1952), "Channelling in packed columns", *Chem. Eng. Sci.*, p. 1.

Homsy, G. (1987), "Viscous fingering in porous media", *Ann. Rev. Fluid Mech.*, Vol. 19, p. 271.

Lajeunesse, E., Martin, J., Rakotmalala, N., Salin, D. and Yortsos, Y.C. (1999), "Miscible displacement in a Hele-Shaw cell at high rates", *J. Fluid Mech.*, Vol. 398, p. 299.

McCloud, K.V. and Maher, J.V. (1995), "Experimental perturbations to Saffman-Taylor Flow", *Physics Reports*, Vol. 260, p. 139.

Manickam, O. and Homsy, G. (1993), "Stability of miscible displacements in porous media with non-monotonic viscosity profiles", *Phys. Fluids A.*, Vol. 5, p. 1356.

Manickam, O. and Homsy, G. (1994), "Simulation of viscous fingering in miscible displacement with non-monotonic viscosity profiles", *Phys. Fluids*, Vol. 6, p. 95.

Manickam, O. and Homsy, G. (1995), "Fingering instabilities in vertical miscible displacement flows in porous media", *J. Fluid Mech.*, Vol. 288, p. 75.

Meiburg, E. and Chen, C.-Y. (2000), "High-accuracy implicit finite difference simulations of homogeneous and heterogeneous miscible porous media flows", *SPE J.*, 5 June, p. 2.

Pankiewitz, C. and Meiburg, E. (1999), "Miscible porous media displacements in quarter five-spot configuration. Part 3, Non-monotonic viscosity profiles", *J. Fluid Mech.*, Vol. 388, p. 171.

Peaceman, D.W. and Rachfird, H.H. (1962), "Numerical calculation of multidimensional miscible displacement", *SPE J.*, December, p. 327.

Petitjeans, P., Chen, C.-Y., Meiburg, E. and Maxworthy, T. (1999), "Miscible quarter five-spot displacements in a Hele-Shaw cell and the role of flow-induced dispersion", *Phys. Fluids*, Vol. 7, p. 1705.

Rogerson, A. and Meiburg, E. (1993a), "Numerical simulation of miscible displacement processes in porous media", *Phys. Fluids A.*, Vol. 5, p. 1344.

Rogerson, A. and Meiburg, E. (1993b), "Numerical simulation of miscible displacement processes in porous media flows under gravity", *Phys. Fluids A.*, Vol. 5, p. 2644.

Ruith, M. and Meiburg, E. (2000), "Miscible rectilinear displacements with gravity override. Part 1: Homogeneous porous medium", *J. Fluid Mech.*, Vol. 420, p. 225.

Saffman, P. and Taylor, G. (1958), *Proc. R. Soc. London Ser. A.*, Vol. 245, p. 312.

Sherwood, J.D. (1987), "Unstable fronts in a porous medium", *J. Comput. Phys*., Vol. 68, p. 485.

Tan, C.T. and Homsy, G.M. (1986), "Stability of miscible displacements in porous media: rectilinear flow", *Phys. Fluids*, Vol. 29, p. 3549.

Tan, C.T. and Homsy, G.M. (1988), "Simulation of nonlinear viscous fingering in miscible displacement", *Phys. Fluids*, Vol. 31, p. 1330.

Taylor, G.I. (1953), "Dispersion of soluble matter in a solvent flowing slowly through tube", *Proc. R. Soc. Lond. A*., Vol. 219, p. 186.

Yortsos, Y. (1990), "Instabilities in displacement processes in porous media", *J. Phys. Condens. Matter*, Vol. 2, p. SA443.